

Supporting information for

**CNT and ZnO Nanorod Incorporated Fish Gelatin Nanocomposite towards Developing
Flexible Pressure/Strain Sensor for Human Motion Monitoring**

Salvin Mustakim¹, Md Abdul Momin², Md Abul Kalam³, Tetsu Mieno^{4,5}, Manisha Ahamad¹,
Mohammad Jellur Rahman^{1*}

¹Department of Physics, Bangladesh University of Engineering and Technology, Dhaka–
1000, Bangladesh

²Department of Bioengineering, Swanson School of Engineering, University of Pittsburgh,
3700 O'Hara St. Pittsburgh, PA 15261, USA

³National Institute of Textile Engineering and Research, Dhaka–1350, Bangladesh

⁴Graduate School of Science & Technology, Shizuoka University, Shizuoka 422–8529, Japan

⁵Department of Physics, Shizuoka University, Shizuoka 422–8529, Japan

* Correspondence: mjrahman@phy.buet.ac.bd

S1. Experimental Section

S1.1. Extraction of FG

Gelatin is extracted from fish scales of Hilsha (*Tenualosa ilisha*) fish, captured from the Padma River, Chandpur, Bangladesh. Initially, the scales are washed thoroughly with tap water to remove impurities and then dried under sun. To eliminate undesired proteins, 100 g of dried scales are treated with 0.1 M NaOH for 1 hour and rinsed with water. The scales are further treated with 10% HCl to remove minerals, followed by washing with water until the pH is neutralized. The chemically processed scales are then vacuum-dried to eliminate moisture. Subsequently, 30 g of the dried scales are placed in 300 mL of deionized (DI) water and heated at 80 °C in a sealed stainless-steel container for 6 hours. After cooling, the mixture is centrifuged at 10,000 rpm for 10 minutes, separating the gelatin from the scales. The supernatant, containing the dissolved gelatin, is poured into a plastic Petri dish and dried to obtain FG. The schematic diagram of this extraction procedure is shown in Fig. S1 ¹.

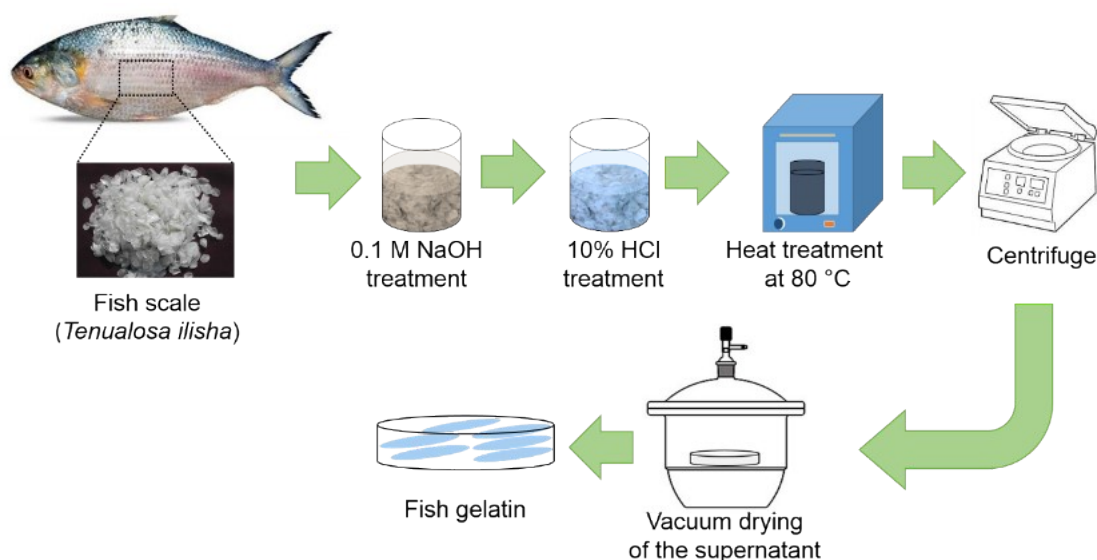


Figure S1. Schematic diagram of the extraction procedure of FG from Hilsha fish scales.

S1.2. Functionalization of CNTs

At first, 50 mg of CNT powder is mixed with 40 ml of pure ethanol and sonicated at room temperature using an ultra-sonic homogenizer (input frequency of 20 kHz and power of 20 W) for 30 minutes. The resulting CNTs/ethanol suspension is then dried and soaked in a 0.15 mole (5 ml) solution of citric acid for over 48 hours. Next, the CNTs in the citric acid solution are placed on the lower electrode of a plasma reactor (0.18 m × 0.15 m), which is evacuated to approximately 0.13 Torr (17.33 Pa) using a rotary pump. Oxygen gas is introduced into the reactor at a controlled rate while maintaining the background chamber pressure at around 0.13 Torr. The plasma reaction is carried out for approximately 15 minutes using an RF input power of 100 W at a frequency of 13.56 MHz. After the plasma treatment, the functionalized CNTs are washed at least three times with DI water and then dried under reduced pressure at room temperature. Next 20 mg of functionalized CNTs are taken into 20 ml DI water and sonicated to prepare CNT–ink. The schematic diagram of the functionalization procedure of CNTs is given in Fig. S2^{2,3}.

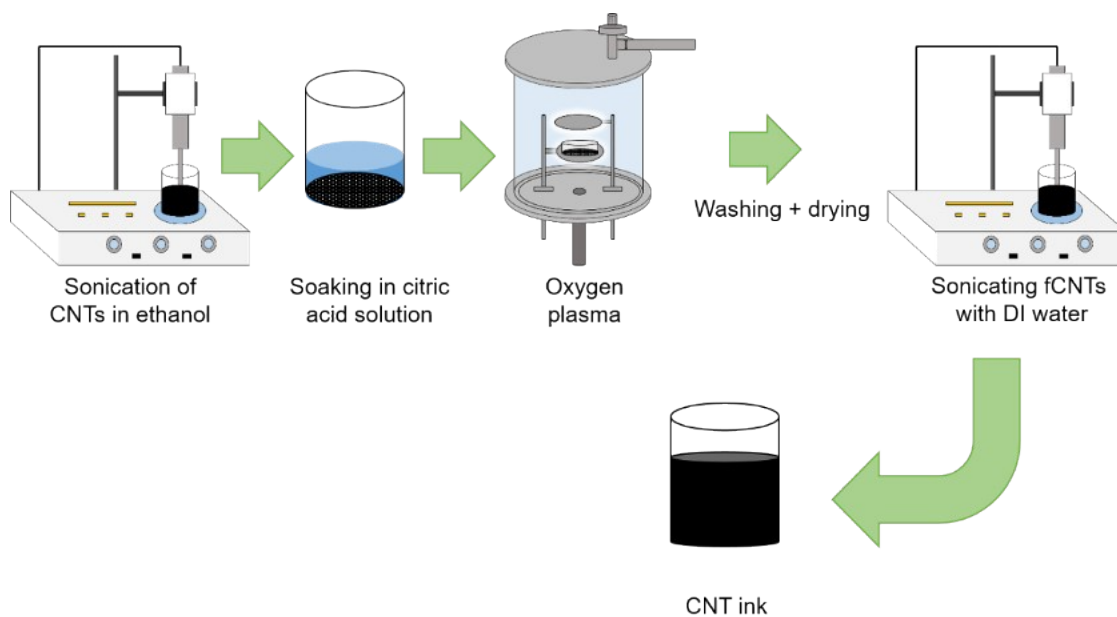


Figure S2. Schematic diagram of the functionalization procedure of CNTs.

S1. 3. Synthesis of the ZNRs

ZNRs are synthesized using a microwave-assisted method in a modified domestic microwave oven. To ensure efficient and uniform heating, the reaction vessel is placed at the hotspot area, slightly to the left of the center of the oven. The sample vessel is connected to a condenser to prevent solvent drying during synthesis. Equimolar solutions of $\text{Zn}(\text{NO}_3)_2 \cdot 6\text{H}_2\text{O}$ and $\text{C}_6\text{H}_{12}\text{N}_4$ are mixed in DI water and stirred. The mixture is then filtered and placed into the microwave oven, operating at a 50% power level. The average synthesis temperature reached $100\text{ }^\circ\text{C}$ after 9 minutes. After completion of the reaction, the white precipitate is washed, centrifuged, and dried⁴. ZnO-NRs are dispersed in water by taking 20 mg in 20 ml DI water, stirring for 1 h at a temperature of $65\text{ }^\circ\text{C}$, and then for 30 min to ensure complete homogenization. This solution of ZnO-NRs is used to prepare the FGCZ nanocomposite. The schematic diagram of the synthesis procedure of ZNRs is given in Fig. S3.

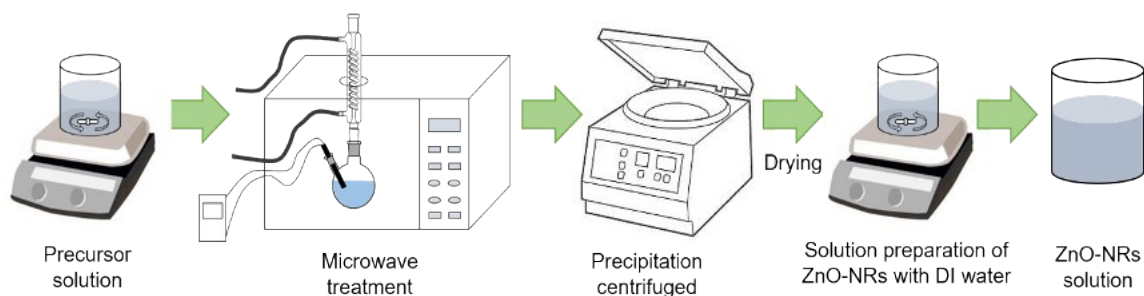


Figure S3. Schematic diagram of synthesis of ZNRs.

S1.4. Fabrication of the FGCZ Nanocomposite

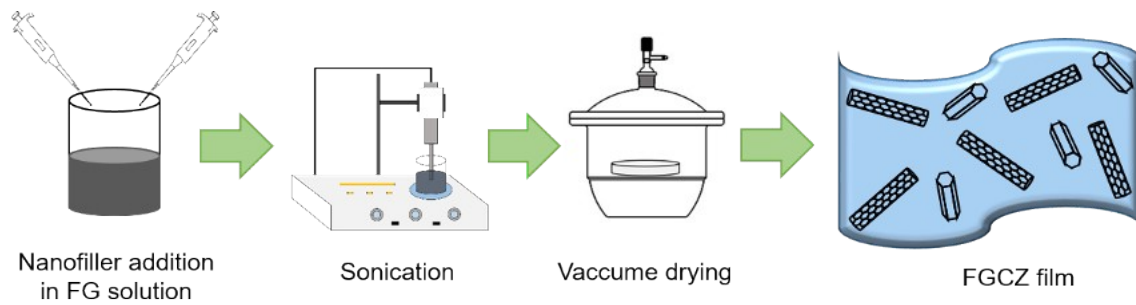


Figure S4 Schematic diagram of the synthesis of FGCZ nanocomposite.

S2. FESEM Images of the Top Surface of the Nanocomposite

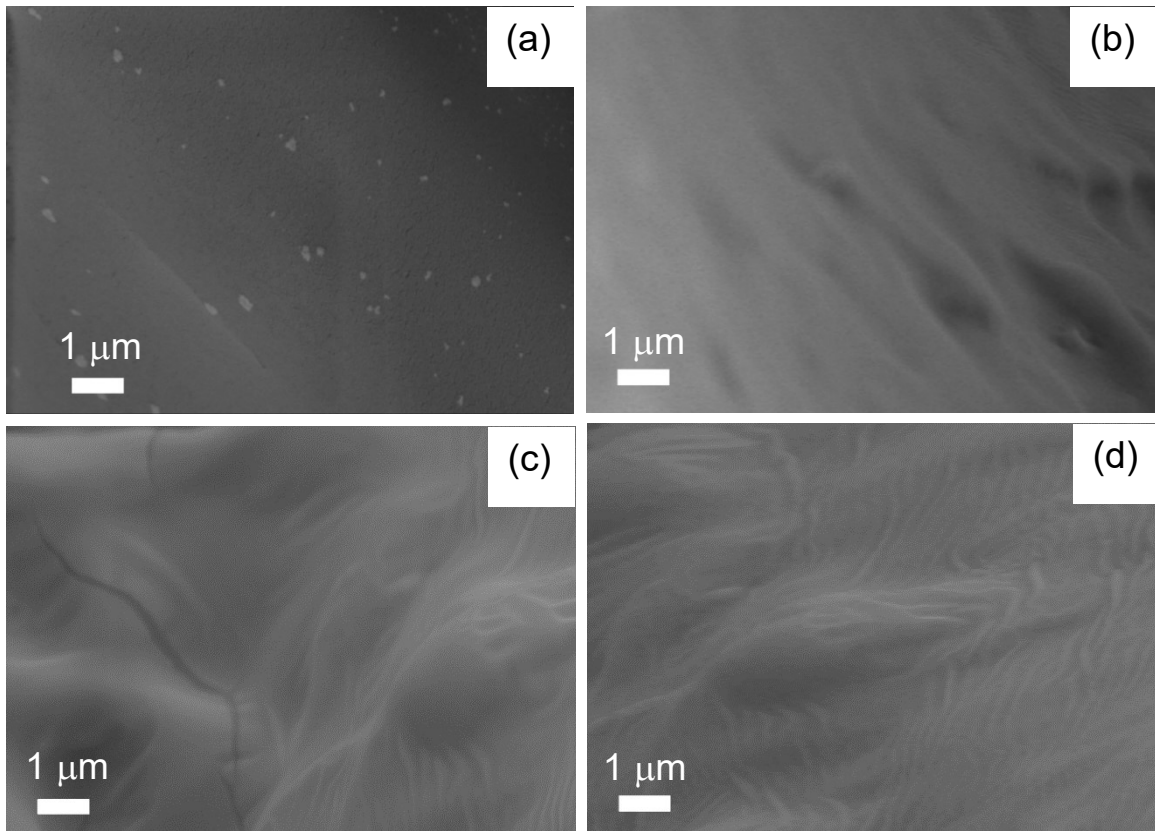


Figure S5. FESEM images of the top surfaces of (a) 0.00% FGCZ (b) 0.20% FGCZ (c) 0.25% FGCZ (d) 0.30% FGCZ.

No nanofillers are visible on the top surface of the nanocomposites.

S3. Computational Method details

Sensing Mechanism

The computational framework for simulating the sensing mechanism of a FG-based composite embedded with CNTs and ZNRs involved a numerical approach to model their distribution, contact point interactions under applied pressure, and the corresponding changes in electrical conductance. The methodology and implementation details are as follows:

Model Geometry and Material Parameters

1. Composite Dimensions:

- The composite was modeled as a cubic volume with dimensions $1 \times 1 \times 1 \text{ mm}^3$.
- The matrix material was FG, with uniformly distributed CNTs and ZNRs.

2. Inclusion Properties:

- Number of CNTs: 5000
- Number of ZNRs: 5000
- CNT dimensions:
 - Length: $100 \mu\text{m}$
 - Diameter: 10 nm
- ZNR dimensions:
 - Length: $100 \mu\text{m}$
 - Diameter: 30 nm

3. Random Position and Orientation:

- Randomly distributed positions and orientations for both CNTs and ZNRs within the FG matrix were generated using a uniform random distribution in 3D space.
- Angular orientations (θ, ϕ) for each inclusion were sampled from a uniform random distribution over 0 to 2π .

Sensing Mechanism Simulation

1. Contact Points Calculation:

- The number of contact points between CNT-CNT, CNT-ZNR, and ZNR-ZNR was computed for a pressure range of 0 to 500 kPa using an exponential scaling model.

$$C_{\text{type}} = C_{\text{max,type}} \cdot (1 - e^{-\beta \cdot P}),$$

where:

- C_{type} : Number of contact points for a given interaction type (e.g., CNT-CNT, CNT-ZNR, ZNR-ZNR).
- $C_{\text{max,type}}$: Maximum contact points for each interaction type (10^6 , 5×10^5 , and 8×10^5 , respectively).
- β : Scaling factor (0.01).
- P : Applied pressure (kPa).

2. Conductance Calculation:

- The overall conductance of the composite was modeled as the sum of all contact points:

$$G = C_{\text{CNT-CNT}} + C_{\text{CNT-ZNR}} + C_{\text{ZNR-ZNR}}.$$

- Conductance was assumed to be proportional to the number of contact points, with higher pressure resulting in increased conductance due to improved connectivity.

Numerical Implementation

1. Distributions:

- CNT and ZNR positions were generated using a uniform random distribution over a cubic matrix of 1 mm^3 .
- Angular orientations were randomly sampled to simulate real-world randomness.

2. Pressure Simulation:

- A pressure range of 0 to 500 kPa was divided into 100 equally spaced intervals.
- For each pressure step, contact points were calculated using the exponential scaling equation.

Visualization

1. 2D and 3D Distributions:

- 2D Visualization: Projected the positions and orientations of CNTs and ZNRs onto the XY plane, with CNTs in red and ZNRs in blue.

- 3D Visualization: Displayed the full spatial distribution of CNTs and ZNRs with their orientations, using distinct colors for each inclusion type.
2. Contact Points vs. Pressure:
 - Plotted the number of contact points (CNT-CNT, CNT-ZNR, ZNR-ZNR) as a function of pressure, showing exponential growth with increasing pressure.
 3. Conductance vs. Pressure:
 - Plotted the total conductance as a function of pressure, showing a near-linear increase due to the summation of contact points.

Computational Method twisting

The computational analysis of the twisted FG-based composite embedded with CNTs and ZNRs was performed using a numerical approach to simulate the deformation and stress distribution under controlled twisting conditions. The details of the computational framework, assumptions, and visualization techniques are described below.

Model Geometry and Parameters

The composite was modeled as a rectangular cuboid with dimensions of **50 mm (length) × 4 mm (width) × 1 mm (thickness)**, consistent with experimental observations. The composite material consisted of a FG matrix embedded with uniformly dispersed CNTs and ZNRs. Two cases of twisting were considered:

1. **Case 1:** Two full twists (720° or $2 \times 2\pi$ radians).
2. **Case 2:** Three full twists (1080° or $3 \times 2\pi$ radians).

The twist deformation was applied along the length of the composite, starting with zero twist at one end and increasing linearly to the specified maximum twist angle at the other end.

Mathematical Representation of Twisting Deformation

The twisting deformation was described mathematically using a linear variation of the twist angle (θ) along the length of the composite. The deformation of each point in the composite was computed using the following transformations:

$$y_{\text{twist}} = y \cos(\theta) - z \sin(\theta),$$

$$z_{\text{twist}} = y \sin(\theta) + z \cos(\theta),$$

where:

- x, y, z : Initial coordinates of a point in the composite.
- $\theta = \theta_{\text{max}} \cdot (x/L)$: Twist angle at a position x , linearly proportional to the composite's length L .
- $y_{\text{twist}}, z_{\text{twist}}$: Twisted coordinates after deformation.

The maximum twist angle (θ_{max}) was $2 \times 2\pi$ radians for the two-twist case and $3 \times 2\pi$ radians for the three-twist case.

Stress Distribution

The stress distribution was simplified as being directly proportional to the local twist angle magnitude ($|\theta|$) at each point along the composite length. This approach provides an approximation of the stress variation across the composite under twisting:

$$\sigma(x) = |\theta|,$$

where:

- $\sigma(x)$: Stress at position x along the composite length.
- $|\theta|$: Magnitude of the twist angle at position x .

This simplification assumes that the stress distribution is dominated by the torsional deformation and does not account for shear or other mechanical interactions.

Numerical Grid and Simulation

A 3D numerical grid was constructed to represent the composite geometry and enable visualization of the deformation and stress distribution:

- **200 points along the length (xxx).**
- **50 points along the width (yyy).**
- **10 points along the thickness (zzz).**

Each grid point was transformed based on the twisting deformation equations, and the stress value at each point was calculated using the proportionality with $|\theta|$.

Visualization

The deformation and stress distribution were visualized using high-resolution plots:

1. 3D Scatter Plot:

- The twisted composite geometry was plotted in 3D with a color map representing the stress distribution (σ).
- The stress was displayed using a "viridis" colormap for clear differentiation of stress intensity.

2. 2D Stress Heatmap:

- A top-down view of the stress distribution was plotted as a 2D contour map.
- The stress variation along the length and width of the composite was visualized.

Both 3D and 2D visualizations were generated for each case (two twists and three twists).

Boundary Conditions

- One end of the composite was fixed, while the opposite end was twisted uniformly to achieve the specified maximum twist angle.
- The twisting deformation was applied under the assumption of linear elastic behavior of the composite material.

Assumptions and Limitations

1. Simplified Stress Model:

- Stress was assumed to be directly proportional to the twist angle, ignoring complex shear stresses or material nonlinearity.

2. Elastic Behavior:

- The composite material was assumed to behave elastically, with no permanent deformation or failure during twisting.

3. Material Homogeneity:

The FG matrix with embedded CNTs and ZNRs was treated as a homogeneously distributed composite, without considering filler-filler interaction

S4. XPS Analysis

The atomic % of the primary elements estimated in the XPS analysis are detailed in Table S1. It is essential to note that XPS is a surface-sensitive technique, and the measured atomic % represents the composition of only the outermost surface.

Table S1. Elemental atomic % for FGCZ nanocomposite of different concentrations.

Elements	Atomic %	
	0.00% FGCZ	0.25% FGCZ
C 1s	63.83	72.35
N 1s	13.22	7.31
O 1s	22.09	17.69
Zn 2p	–	1.12

S5. Determination of the Activation Energy

The activation energy (E_a) is determined using Arrhenius equation as follows.

$$J = J_0 e^{-E_a/kT}$$

$$\Rightarrow \ln J = \ln J_0 e^{-E_a/kT}$$

$$\Rightarrow \ln J = \ln J_0 + \ln e^{-E_a/kT}$$

$$\Rightarrow \ln J = \ln J_0 - \frac{E_a}{kT}$$

E_a is determined from the slope of the $\ln J$ vs. $1000/T$ curve and shown in Fig. S6 and estimated in table S2. The J used to calculate the E_a is measured at 10 V.

Table S2. Estimated values of E_a of FGCZ nanocomposites for different concentrations of nanofillers.

Samples	E_a in eV at 10 V
0.00% FGCZ	1940
0.20% FGCZ	331.84
0.25% FGCZ	185.35
0.30% FGCZ	211.29

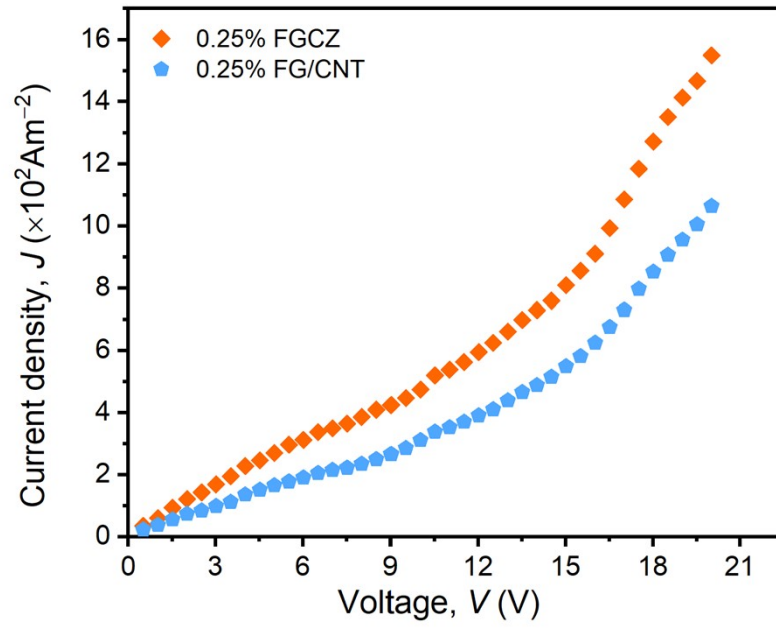


Fig. S6 J-V characteristics of the nanocomposite with and without ZNRs.

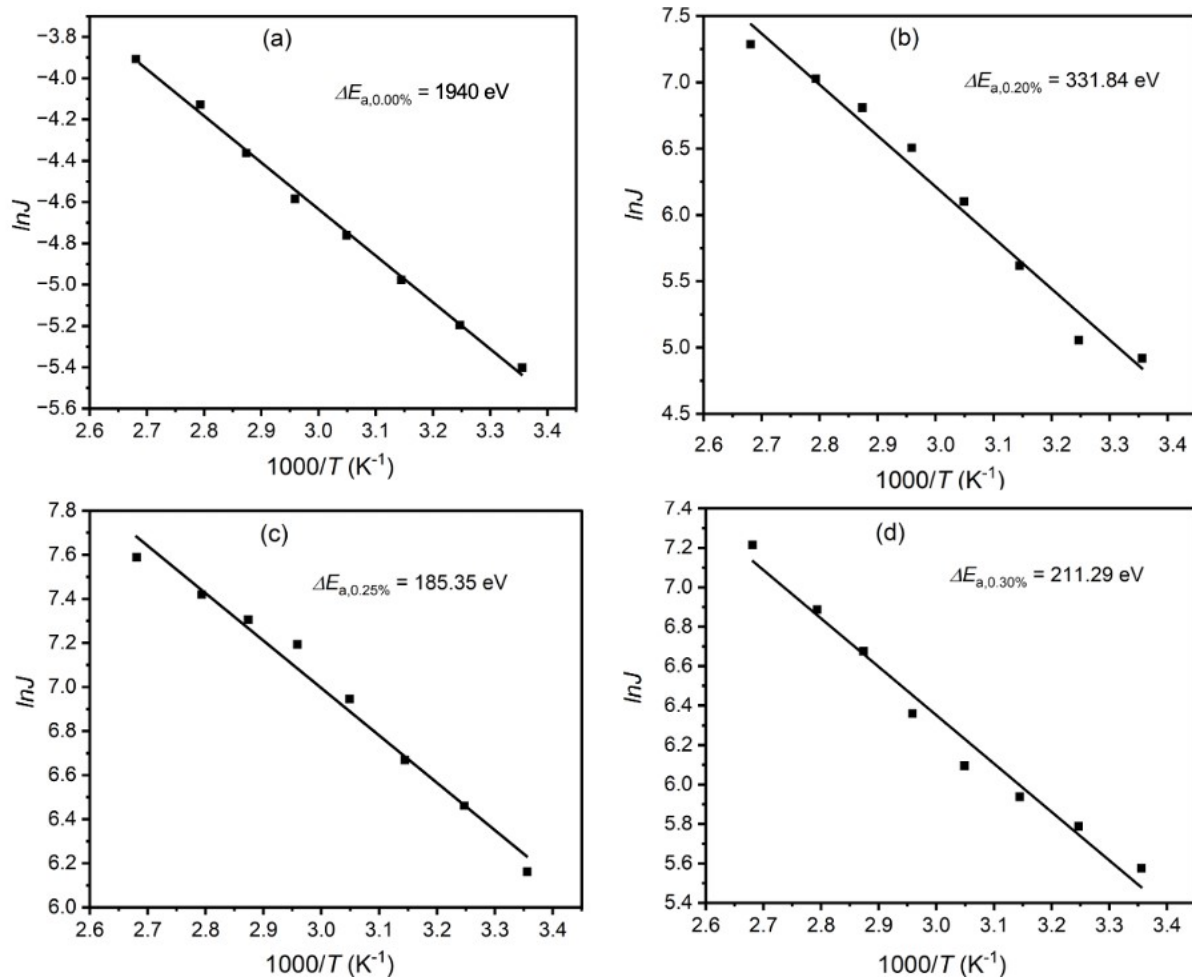


Figure S7. E_a for (a) 0.00% (b) 0.20% (c) 0.25% (d) 0.30% FGCZ nanocomposite.

S6. Sensing Analysis

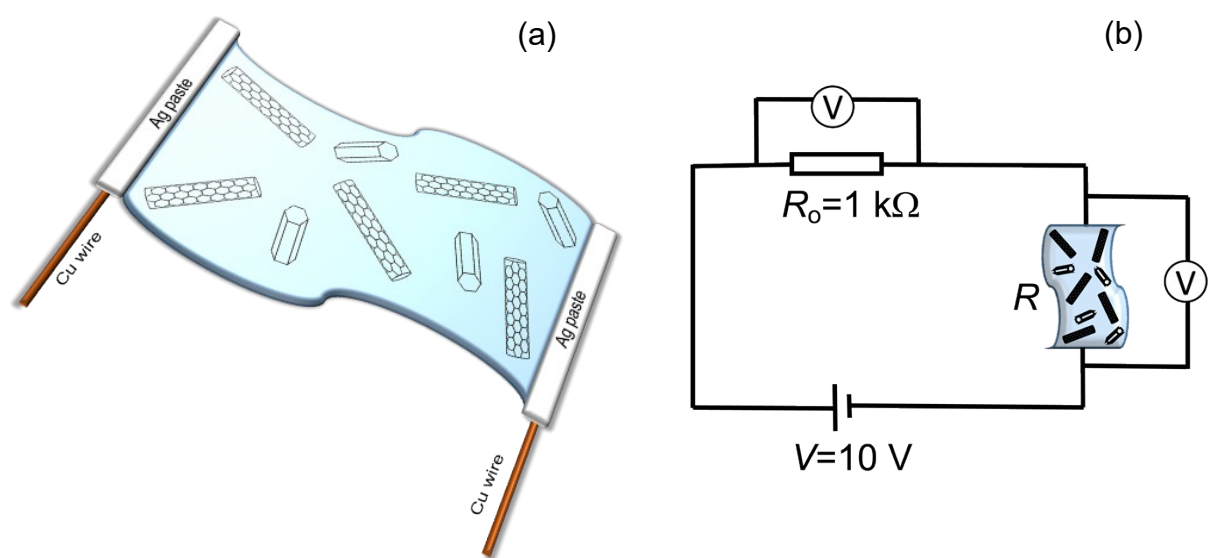


Figure S8. (a) Schematic diagram of the prepared sample and (b) electrical circuit used for sensing measurement.

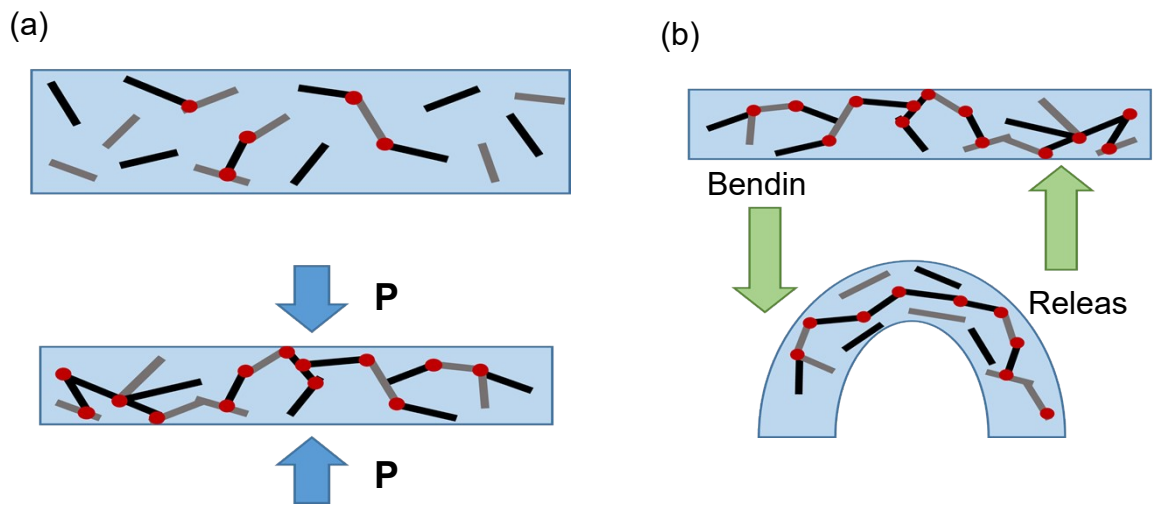


Figure S9. Sensing mechanism of the nanocomposite with applied (a) pressure and (b) strain.

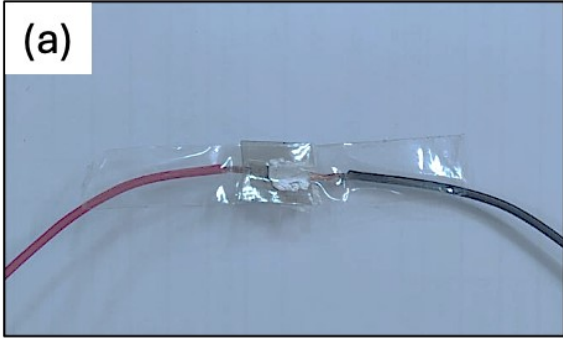


Figure S10. Nanocomposite sensor sealed with Scotch tape.

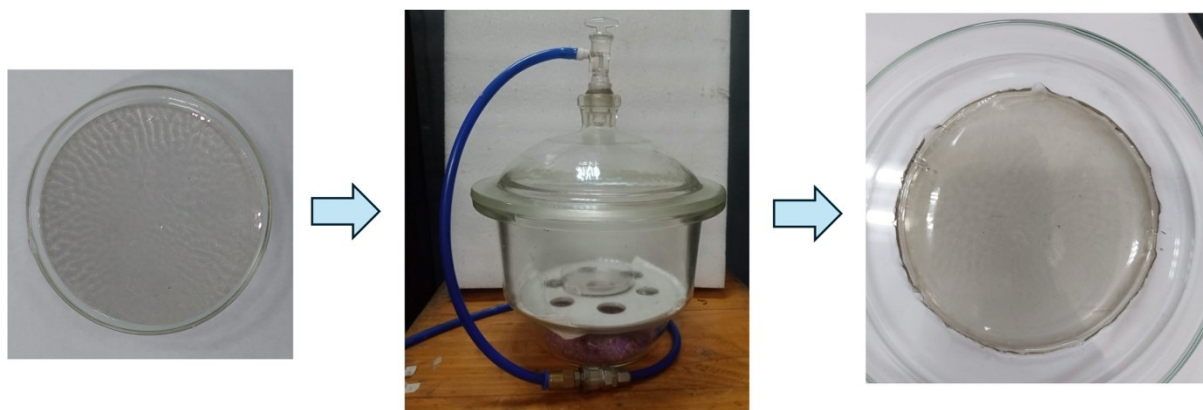


Figure S11. Demonstrating the reproducibility of the nanocomposite by dissolving the film entirely and recasting it.

References

- 1 S. Mustakim, M. A. Kalam, T. Mieno and M. J. Rahman, *ACS Appl Nano Mater*, 2024, **7**, 5202–5213.
- 2 M. J. Rahman and T. Mieno, *J Nanomater*, 2014, **2014**, 508192.
- 3 M. J. Islam, M. J. Rahman and T. Mieno, *Adv Compos Hybrid Mater*, 2020, **3**, 285–293.
- 4 M. Sultana, M. J. Rahman and M. S. Bashar, *J Electron Mater*, 2022, **51**, 2682–2691.